CHAPTER 8

Recent Advances and Prospects in Selective Laser Sintering (SLS) and Melting (SLM) and Multiphoton Lithography for 3D Printing

DYLAN JORALMON, TENGTENG TANG, LAKSHMI JAYANT, MINJU YOO AND XIANGJIA LI*

Department of Mechanical and Aerospace Engineering, Arizona State University, Tempe, AZ 85283, USA.
*Email: xiangjia.li@asu.edu

8.1 Introduction

The research achievements in additive manufacturing (AM), especially in the field of laser 3D printing (L3DP), enable advanced prototyping in terms of speediness and complexity. The laser is used to melt the powder material to form an expected shape; the basic process of L3DP involves spreading a layer of the powder material on a bed with a selected thickness, and the printer runs the laser beam to follow the input trajectory for each layer to print the input shape layer by layer. The build platform adjusts its position when every layer is completed as well to make space for building the part.[1,2] Factors such as the thickness of layers or types of lasers affect the resulting printed materials, including overall resolution or accuracy of the result, speed of manufacturing, or performance of printed parts, since heat is already

Optical, Electronic and Magnetic Materials No. 2
Laser-based Techniques for Nanomaterials: Processing to Characterization
Edited by Nandakumar Kalarikkal, Rodolphe Antoine, Sabu Thomas and Padiyakkuth Nideesh

Published by the Royal Society of Chemistry, www.rsc.org

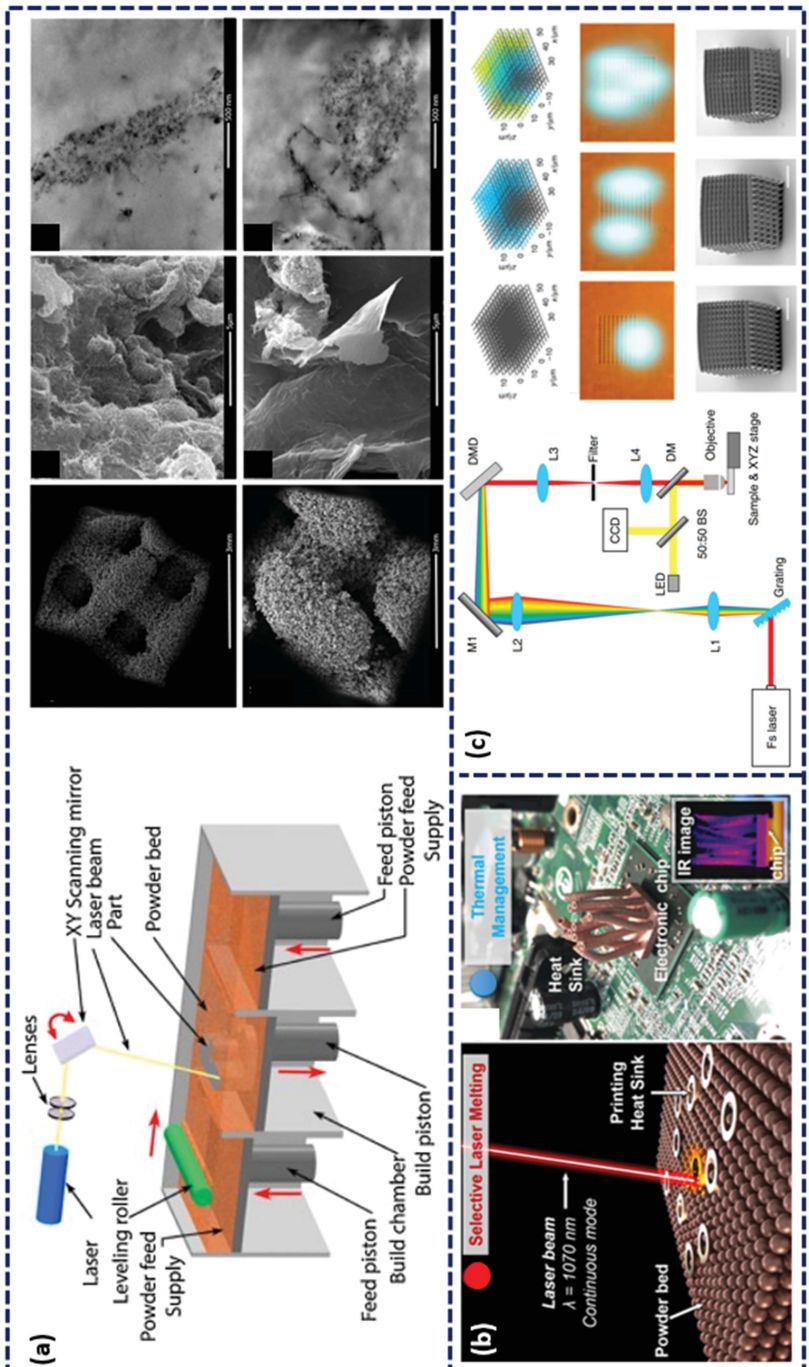
(a)
Lenses
XY Scanning mirror
Laser beam
Part
Powder bed
Laser
Leveling roller
Powder feed
Supply
Feed piston
Build chamber
Build piston
Feed piston
Powder feed
Supply
(b)
Selective Laser Melting
Laser beam
λ = 1070 nm
Continuous mode
Printing
Heat Sink
Powder bed
Thermal
Management
Heat
Sink
Electronic chip
IR image
chip
(c)
DMD
M1
L2
L3
Filter
L4
DM
Objective
CCD
50:50 BS
LED
L1
Grating
Fs laser
Sample & XYZ stage

tapplied during the printing process.[2,3] The most typically used and developed L3DP techniques are selective laser sintering (SLS), selective laser melting (SLM), and multiphoton lithography (MPL) or two-photon polymerization (TPP). The SLS and SLM types share the general process of manufacturing and are both powder bed fusion processes. The main difference between SLS and SLM is the method of combining the powder, creating the printed material, and the features of a printed part following each method. The SLS approach heats the particles of powder material by energy from the laser beam to sinter and fuse with each other before the particles reach their melting point, and the layers combine into the printed part after repeating the procedure of laser drawing input figures of each layer (Figure 8.1a).[4] After the completion of each layer, a new layer of the particles is distributed by a roller while the feed bed moves up and the print bed moves down. The adjustment of bed positions allows the printer to have uniform thickness. SLS printers have the advantages of reusing powder materials that are not sintered during the printing process and reducing steps since they do not use any solvent that evaporates after the printing process.[4,5] On the other hand, the SLM type of 3D printing has a similar manufacturing process of spreading a powder for each layer and selectively fusing or melting it by utilizing a high-power laser. Depicted in Figure 8.1b, the laser path directly runs on the surface of powder materials for each layer, and thermal energy from the laser melts the particles of powder material in a certain thickness and makes them fuse to create the printed part.[6,7] The TPP printer utilizes different methods compared with the SLS and SLM types as it uses photopolymerization of a light-sensitive resin through laser. Even though it also uses a laser to print the object, it is not in the form of powder bed fusion.[8] As shown in Figure 8.1c, TPP-type 3D printers typically incorporate a galvanometric scanner for raster-scan and XYZ stage for axial scanning or sample maneuvering that fabricates the part in a layer-by-layer approach by moving the sample stage axially to polymerize the next layer after completing each layer. It has a limitation for creating complex hollow structures due to the scanning process, yet, it takes advantage of having the highest resolution among the 3DP and the ability to create complex structures for the photonic and nanoscale fields.[9] The application of SLS, SLM, and TPP printing techniques is not limited to creating prototypes or models: recent research has

Figure 8.1 Overview of laser AM technologies (a) selective laser sintering (SLS) printing schematic illustrating powder coating and scanning strategies to fabricate 3D metal objects with small features. Reproduced from ref. 10, https://doi.org/10.3390/polym12081841, under the terms of the CC BY 4.0 license, https://creativecommons.org/licenses/by/4.0/, and from ref. 15 with permission from Elsevier, Copyright 2017. (b) Laser scanning strategies to obtain desired microstructure of fused nanocomposite material. Reproduced from ref. 16 with permission from Elsevier, Copyright 2020. (c) TPP schematic and fabrication of micro lattices. Scale bars are 10 μm. Reproduced from ref. 9, https://doi.org/10.1038/s41467-019-10249-2, under the terms of the CC BY 4.0 license, http://creativecommons.org/licenses/by/4.0/.

expanded the possibilities of the application to the energy, electronic, photonic, and biomedical industries. Rollo *et al.* conducted research on fabricating porous conductive 3D structures by using SLS; this demonstrates the development of the SLS manufacturing technique actualizing the creation of conductive polymer composites with complex geometric features including porosity and void size.[10] The research by Naujokat *et al.* indicates an impact of SLM technology in the biomedical field—SLM with shape-memory alloys for intraosseous and subperiosteal implants having sufficient biocompatibility.[11] Other research on SLM has established its reliability in nanocomposites, SLM is employed to tune the crystallographic structure and nanocomposite for electrochemical energy conversion and storage systems. The method of SLM improves the resolution and mechanical properties of printed parts.[12] TPP printing, based on the multiphoton polymerization of a transparent photopolymer, has established its advantages in the photonic field because it has high resolution that allows the freeforming of micro-optical elements and components including complex lenses and metalenses/metasurfaces with supporting optimization for nanophotonic lens design due to not having chemical processes.[9,13,14] In the process of TPP, the laser solidifies the resin in nanoscale blocks, such as voxels, since it is focused on a highly confined region within a photosensitive resin which induces nonlinear absorption. It enables TPP to process a wide range of applications of nanostructures including photonic crystals.[9]

8.2 Selective Laser Sintering

8.2.1 Overview of Selective Laser Sintering

Selective laser sintering (SLS) is a powder bed fusion AM approach that incorporates a scanning laser to selectively sinter fine powders into a solid part with morphology defined by a computer model.[4] After each individual layer is solidified, a powder roller uniformly distributes fresh powder to be subsequently sintered by the scanning laser until the printed part is completed. In order to adequately sinter adjacent particles, the sintering kinetics, including necking radius, are investigated to optimize the printing parameters, resulting in high resolution and control of the dimensions and microstructure of the printed part.[17] The three mechanisms of particle sintering include partial fusion, complete fusion, and chemical bond fusion. Printing parameters, including the laser power and scanning speed, can be modulated to produce porous or dense microstructures using nanocomposite materials for advanced electronics, biological sensors, and thermal management devices.[2] SLS-printed devices can be fabricated into unique geometries that are otherwise costly or difficult to produce using conventional methods, such as slip casting or hot isostatic pressing.[18] In the following subsections, recent developments to address ongoing challenges for fabricating polymer and ceramic composites through SLS and current nanomaterials of interest to the scientific community are elaborated. The section concludes with a brief discussion of recent applications of nanocomposites in the field of biomedicines, aerospace, and electronics.

8.2.2 Selective Laser Sintering Process and Development

SLS and selective laser melting (SLM) share a fundamental process principle known as powder bed fusion and thus it is crucial to distinguish between these two techniques. The primary distinction between SLS and SLM lies in their approach to the powder to be fused during printing.[19] SLS techniques form the 3D objects using laser energy to heat powder particles, to their relative sintering temperature, to facilitate fusion between them to create a solid structure. The SLS system consists of three main parts: a spreading platform, a powder bed, and a laser system with a laser and scanner. The powder is evenly spread on the building platform using a slot feeder and a roller or scraper blade to level the surface and ensure uniformity amongst the powders within the bed. The system processes the 3D components as planes, with each plane representing basic laser scanning elements known as vectors. The scan pattern of these vectors is predetermined based on the desired morphology and dimensions of the final product. The material is heated below its melting point, causing fusion between particles through laser sintering or melting. The scanner directs the laser to move in a two-dimensional plane while adjusting the powder bed's height to focus the laser on the newly formed surface (Figure 8.2a).[20] After each layer, the powder bed is lowered by one layer thickness, and a new layer of powder is deposited and fused by the laser. This cycle continues until the entire object is built. The completed product cools down inside the printer once construction is finished.[19] As depicted in Figure 8.2b, different analysis methods, for studying the sintering of particles during the energy deposition process, have been investigated to optimize printing parameters.[17] *In situ* X-ray imaging shows the influence of laser power and sintering time on the necking radius of the particles, which is critical for controlling the resolution of the printed particles.[17] This leads to appealing potential to tailor the microstructures of emerging nanocomposites to alter the performance through anisotropic structures. For example, drug delivery devices for biomedicine can be manufactured using SLS and the drug packing for individual tablets can be accurately controlled by changing porosity of the microstructure by modulating the laser scanning speed, (Figure 8.2c).[21] Mathematical models can be constructed for these materials to predict the level of porosity within the material. Consequently, SLS is a facile approach with increasing applications in the aerospace, bioelectronics, and defense industries.[5,22]

8.2.3 SLS Nanomaterials and Composites

Selective laser sintering of nanocomposites involves polymer and ceramic composites that integrate nanofiller material to enhanced material properties with the objective of developing printed parts with high mechanical strength, increased dielectric behavior, and electromagnetic shielding. Different approaches, such as differential scanning calorimetry, are implanted to study the sintering mechanisms, during heating and cooling, before

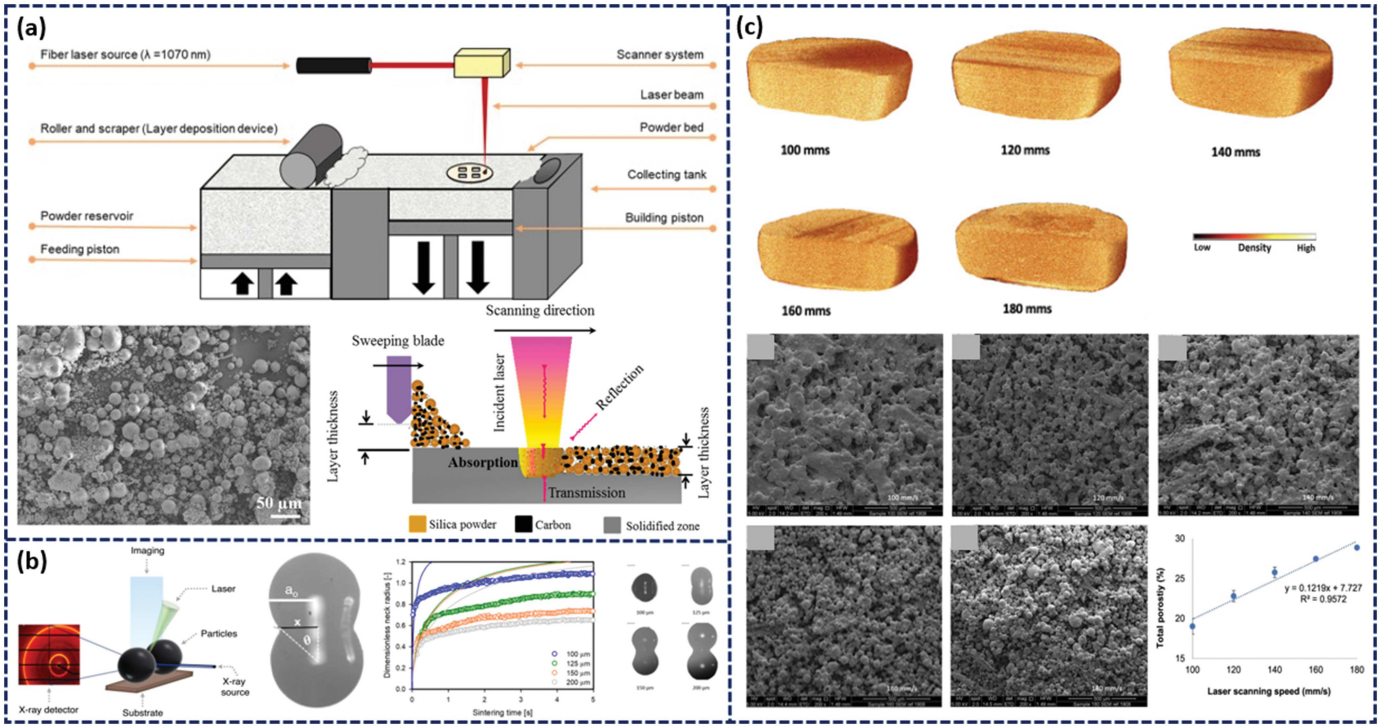

Figure 8.2 Overview of SLS printing technology (a) selective laser sintering (SLS) printing schematic illustrating scanning of individual layer and powder solidification mechanism. Reproduced from ref. 20, https://doi.org/10.1016/j.addma.2021.102542, under the terms of the CC BY 4.0 license, https://creativecommons.org/licenses/by/4.0/, and from ref. 23, https://doi.org/10.3390/ma10111313, under the terms of the CC BY 4.0 license, https://creativecommons.org/licenses/by/4.0/. (b) *In situ* monitoring of PA12 particle sintering at different sintering times. Reproduced from ref. 17, https://doi.org/10.1016/j.addma.2022.102624, under the terms of the CC BY 4.0 license, https://creativecommons.org/licenses/by/4.0/. (c) Evaluation of porosity and microstructure *via* SEM in drug release tablets at different scanning speed. Reproduced from ref. 21, https://doi.org/10.1016/j.ijpx.2022.100148, under the terms of the CC BY 4.0 License, https://creativecommons.org/licenses/by/4.0/.

Table 8.1 Summary of recent progress in selective laser sintering. CNT, carbon nanotubes; TPU, thermoplastic polyurethane; PA, polyamide; MWCNTS, multi-walled carbon nanotubes; SiNW, silicon nanowires; EMI, electromagnetic interference.

Study	Method	Material	Laser power	Minimum feature size	Laser scanning speed	Application
Zhou *et al.*[18]	SLS	CNT–TPU	11.5–20.5 W	100 μm	3000 mm s^{-1}	Flexible electronics and sensors
Qi *et al.*[28]	SLS	PA11/$BaTiO_3$/CNT	7.5 W	~200 μm	7600 mm s^{-1}	Dielectric materials
Song *et al.*[25]	SLS	PVDF/graphene	40 W	~300 μm	7600 mm s^{-1}	Piezoelectric materials
Chen *et al.*[24]	SLS	PA12-graphene	21 W	~250 μm	2500 mm s^{-1}	Automotive and textile industry
Yuan and Yu[31]	SLS	PA12-CNT	50 W	~200 μm	2000–4000 mm s^{-1}	Automotive and aerospace
Ding *et al.*[26]	SLS	TPAE–MWCNTS	20 W	~150 μm		Flexible strain sensors
Taher *et al.*[32]	SLS	PA6–CNT	5–15 W	~75 μm	1000–2000 mm s^{-1}	High strength and lightweight
Gomez-Rodriguez *et al.*[29]	SLS	Al_2O_3–Mo	79.5 W		1.25 mm s^{-1}	High strength refractory materials
Yu *et al.*[33]	SLS	SiC–Si_3N_4	18 W	~200 μm	3600 mm s^{-1}	EMI shielding
Wang *et al.*[34]	SLS	Biomass–SiNW/SiC	7 W	~100 μm	2000 mm s^{-1}	EMI shielding
Lanzl *et al.*[35]	SLS	PA12-Cu	16.3 W	~200 μm	1900 mm s^{-1}	Thermal management devices

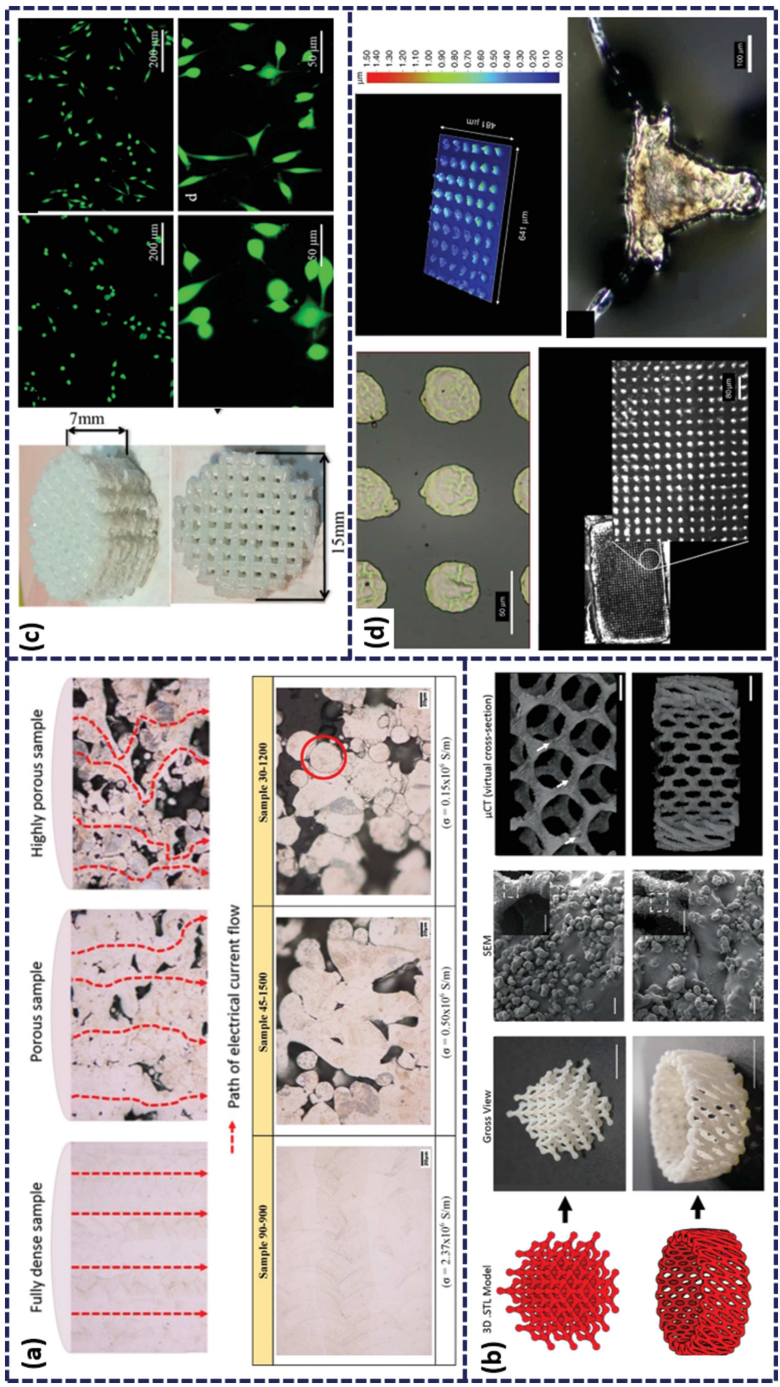
(a)
Fully dense sample
Porous sample
Highly porous sample
Path of electrical current flow
Sample 90-900
Sample 45-1500
Sample 30-1200
(σ = 2.37x10⁵ S/m)
(σ = 0.50x10⁵ S/m)
(σ = 0.15x10⁵ S/m)
(b)
3D STL Model
Gross View
SEM
μCT (virtual cross-section)
(c)
7mm
15mm
200 μm
50 μm
(d)
50 μm
481 μm
641 μm
μm
100 μm

printing which promotes interesting potential nanomaterials to be used with the SLS process. The nanomaterials include different forms of polyamide (PA), polyvinylidene fluoride (PVDF), and thermoplastic polyamide elastomer (TPAE) with nanoparticles such as carbon nanotubes and graphene plates absorbed onto the surface of the PA particles through dry- or melt-mixing.[24–26] The addition of carbon in PA nanomaterials has been demonstrated to result in a significant improvement in mechanical properties and to mitigate fracture of printed parts under tensile, compressive, and three-point bending loads.[24] Furthermore, an extensive exploration of fiber and glass bead reinforcements for SLS nylon composites has underscored the nuanced effects of reinforcement geometry, volume fraction, and material properties on mechanical performance and processing characteristics.[27] Ceramic nanofillers, such as $BaTiO_3$, have been combined with PA and carbon material to generate a percolated network that exhibits superior piezoelectric behavior with good printability.[28] Ceramic metal composites have also been manufactured using the SLS approach, including alumina molybdenum with high fracture toughness for economic refractory materials under flexural loads.[29] For high thermal conductivity ceramic foams where the consideration of thermal diffusion coefficient and specific heat capacity are required, it has been demonstrated that porous mullite ceramics can be fabricated through SLS processes.[30] The almost limitless design geometries facilitated by SLS fabrication, combined with functional nanomaterials, open new pathways to generate more effective biomedical devices, refractory materials, and electronics with excellent performance (Table 8.1).

8.2.4 Application

This section provides a comprehensive explanation of the SLS process, elucidating its utilization of high-energy lasers to sinter sequential layers of powder, enabling the creation of intricate 3D structures for a myriad of engineering applications. It emphasizes the precision, complexity, and potential of SLS in synthesizing composite materials into functional devices. As shown in Figure 8.3a, the influence of laser scanning power and speed can

Figure 8.3 Recent applications in SLS-based printing approaches: (a) comparison of microstructure in SS316L printed specimens at different scanning speeds. Reproduced from ref. 36 with permission from Elsevier, Copyright 2016. (b) SLS-printed lattice structures with inset SEM images. Scale bars are 1 cm, 1 mm, 100 μm inset, and 3 mm from left to right. Reproduced from ref. 37, https://doi.org/10.1371/journal.pone.0147399, under the terms of the CC BY 4.0 license, https://creativecommons.org/licenses/by/4.0/. (c) TTCP bone scaffold with immunofluorescence imaging after 6 hours and 12 hours. Reproduced from ref. 38, https://doi.org/10.3390/ma13102268, under the terms of the CC BY 4.0 license, https://creativecommons.org/licenses/by/4.0/. (d) Array of circles of sintered silver nanoparticles (AgNP) and bull logo with microscale resolution. Reproduced from ref. 39, https://doi.org/10.1038/s41378-019-0116-8, under the terms of the CC BY 4.0 License, https://creativecommons.org/licenses/by/4.0/.

produce high porosity in stainless steel 316 specimens.[36] Consequently, the conductivity of each sample can be adjusted since the number of mean pathways for ions to conduct through decreases significantly for the porous sample when compared with the dense microstructure. SLS printing has prevailed in the field of biomedicine because it can reproduce intricate morphologies, such as diamond or diagrid lattices, for bone tissue regeneration studies with polycaprolactone and subsequent vapor smoothing (Figure 8.3b).[37] This approach is especially useful due to the high demand for customized parts with increased compression strength and biocompatibility for regenerative medicine.[37,38] As mentioned previously, different nanofillers can be incorporated into the matrix to reinforce the material, however the cytocompatibility would need to be investigated in order for them to be implemented into medicinal applications. As shown in Figure 8.3c, bone scaffolds comprised of tetracalcium phosphate (TTCP) show good cell viability after 12 hours and compressive strengths up to 11.87 MPa making this advantageous for medicine since TTCP is biodegradable.[38] Ceramic nanofillers have also been utilized by infusing silicon nanowires (SiNWs), with a matrix of biomass from cedar trees, to fabricate metastructures with improved electromagnetic shielding capabilities at −49.01 dB at a frequency of 5.1 GHz.[34] Recent development into the micro resolution capabilities of SLS printing technologies has led to the integration of a digital micromirror device, a complex array of tiny mirrors to reflect an image, and a SLS-scanning laser to selectively sinter a projection area in contrast to a tool path approach for microelectronics.[39] An array of silver nanoparticles are sintered with great dimension control and can be printed in an instant and microelectronics are producible with a minimum feature size of less than 7 μm, see Figure 8.3d.[39] Therefore, the potential applications of SLS-printed ceramic and polymer composites show promising alternative manufacturing methods for next-generation electronics and advanced ceramics.

8.3 Selective Laser Melting

8.3.1 Overview of Selective Laser Melting

Selective laser melting (SLM) is a laser additive manufacturing approach, similar to selective laser sintering, that utilizes a high-power scanning laser and optics system to selectively heat predetermined regions of powders, converting the powders into a molten state that subsequently solidifies to form a portion of the final printed part.[40,41] In contrast to selective laser sintering, where the particles are fused together by heating the particles to their relative sintering temperatures, powders are melted and cooled by heat transfer mechanisms to form dense metal structures from a digital model.[42] This facile approach is advantageous since the scanning laser power can be attenuated to alter the microstructure of different metal and nanofiller powder-based materials for physical property enhancement.[43,44] Additionally, it is imperative to consider the influence of printing parameters, such as

melt pool dynamics and printing speed, on the overall resolution, dimensional accuracy, and thermally induced defects of each individual layer in the printed part to meet tolerance requirements.[42,45,46] Because SLM technologies have exhibited the ability to print different metal alloys and nanocomposite materials, there has been an increased interest in extending this manufacturing tool towards the design of functional devices with applications in the automotive, chemical, and aerospace industries.[44,46,47] In the following subsections, the working principle of SLM printing and recent developments in material selection and physical property enhancement utilizing SLM nanocomposite 3D printing are elucidated. Furthermore, present-day applications of SLM printed nanocomposite devices are highlighted.

8.3.2 Selective Laser Melting Process and Development

Selective laser melting AM technologies are energy-deposition-based AM technologies that employ galvanometer mirrors and a high-power laser system to selectively melt a metal matrix composite into a geometric design defined by a computer model. The main distinguishing feature of SLM printing from SLS is that the uniformly distributed powders are heated to their melting temperature of the nanomaterial and the particles are cooled through convection, radiation, and conduction heat transfer mechanisms (Figure 8.4a).[42,48] The powders are mixed with nanofiller material and milled to achieve a uniform particle size distribution to aid in both the fusion and recoating process.[49] The nanomaterial is distributed into the powder bed, under specific atmospheric conditions, and the laser travels along the powder surface, spaced out by the hatch distance, to solidify each individual layer of the digital model. The powder bed is then incrementally moved by the defined layer thickness and recoated evenly by a high precision roller for all of the individual layers to fabricate the desired nanocomposite structure. Furthermore, it is imperative that the scanning power and linear speed parameters are adjusted in order to dictate the melt pool thermodynamics to enhance the fusion of adjacent powders within the powder bed.[50] High power lasers spontaneously deposit a large amount of energy onto the surface of the powder and the subsequent fusion process, coupled with the linear motion of the laser, can result in particle ejection and defects within the microstructure.[50] Consequently, the influence of printing parameters on microstructure development during SLM must be closely evaluated to meet the demands of emerging metastructures with increased mechanical strength and thermal conductivity. Numerous scanning strategies have been explored in order to achieve different microstructures with anisotropic physical properties. For example, melting with recoating mechanisms generate porous microstructures while remelting scanning results in a dense microstructure with high relative density (Figure 8.4b).[51] Remelting scanning approaches can reorient themselves, passing the small area multiple times at different scanning angles, to influence the grain structure of the

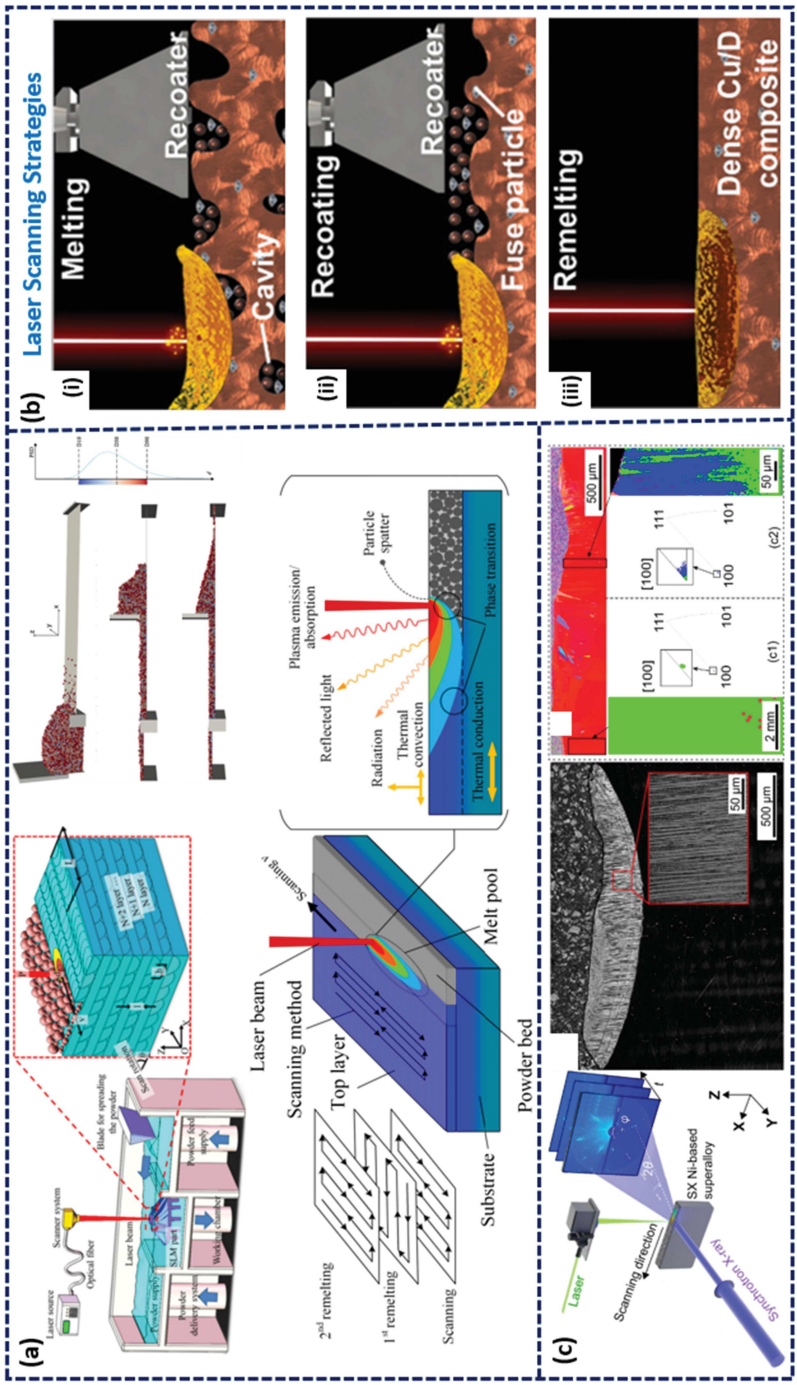
(a)
Laser source
Scanner system
Optical fiber
Laser beam
SLM part
Powder supply
Powder delivery system
Blade for spreading the powder
Powder side supply
Workpiece chamber
Laser beam
Scanning method
Top layer
Melt pool
Substrate
Powder bed
Scanning
1st remelting
2nd remelting
Plasma emission/ absorption
Reflected light
Radiation
Thermal convection
Thermal conduction
Particle spatter
Phase transition
(b)
Laser Scanning Strategies
(i)
Melting
Recoater
Cavity
(ii)
Recoating
Recoater
Fuse particle
(iii)
Remelting
Dense Cu/D composite
(c)
Laser
Scanning direction
SX Ni-based superalloy
Synchrotron X-ray
500 μm
50 μm
2 mm
(c1)
(c2)
[100]
111
100
101

final printed part. The unique ability to adjust the microstructures by simply adjusting the laser power and scanning strategy opens up new perspectives in the design of high entropy alloys (HEAs) and metal and ceramic matrix composites for components designed to withstand harsh environmental conditions. Developments in real time dynamic analysis of the melt pool dynamics have increased the single crystalline parts of Ni-based super alloys printed by SLM through X-ray Laue diffraction experiments (Figure 8.4c).[52] The real time evaluation of the microstructure development of new superalloys and high entropy alloys provides intriguing perspectives on tunable hierarchical microstructures for emerging high strength and lightweight SLM printed components.

8.3.3 SLM Nanomaterials and Metal Matrix Composites

In order to meet desired mechanical and thermal performance requirements, the material selection and powder processing approach is a decisive step when fabricating robust metal matrix composites *via* the SLM process. Metal matrix composites and metal alloys powders are ball milled at high speeds to achieve a homogenous mixture of spherical particles tailored to a specific overall size distribution.[53,54] Furthermore, cost effective, lightweight metal nanocomposites can be fabricated through the SLM process into complex geometries, unseen in traditional manufacturing methods, to develop next-generation functional nanocomposite devices with excellent material properties.[50,55] Selective laser melting nanocomposites largely incorporate advanced nanocomposite powders which include alumina as nanofiller matrix within an aluminum matrix for mechanical reinforcement in extreme environments seen in the automotive and aerospace industries.[53,56] Furthermore, the development of novel high entropy alloys has grown significantly because of their attractive strength and ductility, which can be improved through the addition of dual phase face-centered and body-centered cubic structures, resulting in higher yield strengths.[41,57] Laser scanning parameters can be adjusted to produce hierarchical

Figure 8.4 Working principle of current SLM printing technologies. (a) Selective laser melting (SLM) printing schematic illustrating powder coating, scanning strategies, and melt pool thermodynamics. Reproduced from ref. 48, https://doi.org/10.3390/ma15207049, under the terms of the CC BY 4.0 license, https://creativecommons.org/licenses/by/4.0/, from ref. 49 with permission from Elsevier, Copyright 2019, and from ref. 50, https://doi.org/10.3390/ma12050720, under the terms of the CC BY 4.0 license, https://creativecommons.org/licenses/by/4.0/. (b) Laser scanning strategies to obtain desired microstructure of fused nanocomposite material. Reproduced from ref. 51 with permission from Elsevier, Copyright 2021. (c) Evaluation of melt pool dynamics and microstructure development of Ni-based superalloy *via* X-ray synchrotron projection. Reproduced from ref. 52, https://doi.org/10.1038/s41467-023-38727-8, under the terms of the CC BY 4.0 License, https://creativecommons.org/licenses/by/4.0/.

microstructures, demonstrating that the density and porosity can be tuned to acquire materials with different tensile and deformation properties.[58] A recent study investigated the printability and electrical properties of AlSi10Mg nanoparticles with dispersed CNT nanomaterial as functional filler material to facilitate improved mechanical properties, such as tensile strength and ductility.[59] In general the nanofiller's properties can be utilized to augment the physical properties and microstructure of the metal matrix. For example, electrochemical and corrosion resistant materials have gained increased attention since the addition of MoS_2, into a pure Mo matrix, can inhibit crack formation from residual stresses while also achieving high electrochemical performance required for modern sodium-ion energy applications.[60] Moreover, biocompatibility and biodegradation is a critical factor for exploring materials with biomedical applications and recent evaluation of a Fe–Mn alloy demonstrated excellent cytocompatibility with high mechanical strength for tissue repair applications.[61] Consequently, the vast library of available metal and ceramic nanocomposite materials printed *via* SLM is continuously expanding horizons, offering unparalleled mechanical strength, thermal conductivity, and corrosion resistance for physically demanding applications in the most extreme environments (Table 8.2).

8.3.4 Applications

Recent advancements in SLM laser optics and powder processing have led to an increased capacity to fabricate intricately designed devices, with macroscale to microscale features, from nanocomposite materials with increased corrosion resistance, mechanical reinforcement, and enhanced heat dissipation.[50,54] Since the printed structures can withstand the most extreme environments, this opens up new potential metal composite designs for aerospace and defense applications that operate at high temperatures and pressures. Murray *et al.* presented a CoNi super alloy, fabricated either through SLM or electron beam melting (EBM) techniques, exhibiting dense grains and tensile strength of approximately 1.1 GPa and superior ductility when compared with current Ni-based superalloys printed *via* SLM (Figure 8.5a.)[64] The addition of Co into the Ni matrix allows for the fabrication of complex CoNi super alloy including turbine blades with intricately designed cooling channels that increase the overall engine efficiency and robustness.[64] Similarly, a novel CuCrZr powder was fabricated *via* SLM into microlattice structures by Ma *et al.* and the plasticity and energy absorption properties were enhanced while maintaining high thermal and electrical conductivity (Figure 8.5b).[70] The lattice structure size and volume fraction can be altered in the computer design model to acquire CuCrZr alloy materials with different compression strengths ranging from 1.84 to 12.83 MPa.[70] These lightweight lattice structures are advantageous for biomedical implants and bone scaffolds for tissue repair that require high strength materials that have good biocompatibility, depicted in Figure 8.5c.[71] A high

Table 8.2 Summary of recent progress in selective laser melting. iHEA, interstitial solute-strengthened HEA; HX, Hastelloy X; GO, graphene oxide.

Study	Method	Material	Laser power	Minimum feature size	Laser scanning speed	Application
Jiang *et al.*[59]	SLM	AlSi10Mg–CNT	350 W	~105 nm	900–1900 mm s^{-1}	High tensile strength and improved electrical conductivity
Zhu *et al.*[55]	SLM	FeMnCoCrC (iHEA)	180 W	~50 μm	1000 mm s^{-1}	Aerospace and automotive
Hu *et al.*[62]	SLM	TiC–HX	200–500 W	~40 μm	500 mm s^{-1}	Wear resistance and mechanical strengthening
Yao *et al.*[56]	SLM	IN718/TiC	300 W	~130 μm	800 mm s^{-1}	Strengthened and oxidation resistant metals
Golyshev *et al.*[63]	SLM	Ti-6Al-4V/-B_4C	95–260 W	~70 μm	330–900 mm s^{-1}	Wear resistance
Dargusch *et al.*[61]	SLM	Fe–Mn	125 W	~75 μm	NA	Hard tissue repair
Murray *et al.*[64]	SLM	Co–Ni	134–176 W	~80 μm	744–1137 mm s^{-1}	Nuclear and energy industries
Baroutaji *et al.*[65]	SLM	AlSi10Mg	370 W	~200 nm	1300 mm s^{-1}	Heat exchangers and impact tolerant structures
Zhang *et al.*[50]	SLM	NbMoTaW (HEA)	500 W	~100 μm	250 mm s^{-1}	Load bearing structures at high temperature
Kang *et al.*[66]	SLM	WC-18Ni-300S	275 W	NA	1360 mm s^{-1}	High strength molds
Xin *et al.*[67]	SLM	Ag–Cu/diamond	40–120 W	~100 μm	400–2000 mm s^{-1}	High hardness and low thermal expansion coefficient
Alinejadian *et al.*[60]	SLM	Mo/MoS_2	25–75 W	~45 μm	65–350 mm s^{-1}	Sodium-ion energy devices and semiconductors
Davydova *et al.*[68]	SLM	Co–B_4C	50–70 W	~70 μm	100–300 mm s^{-1}	Cutting tools
Wen *et al.*[69]	SLM	GO–S136	200 W	~100 μm	900 mm s^{-1}	Harsh corrosion environments

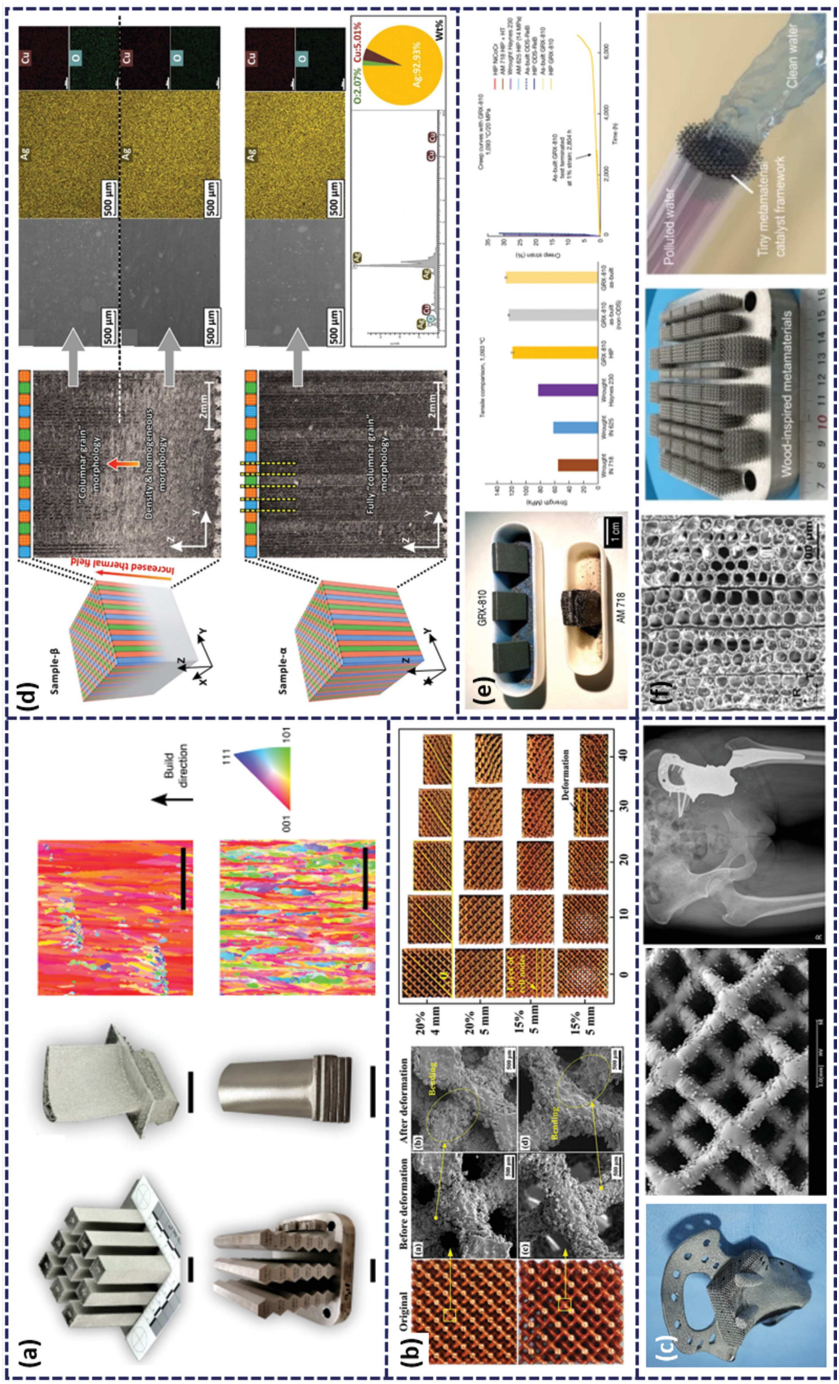
(a)
Build direction
111
101
001
(b)
Original
Before deformation
After deformation
20% 4 mm
20% 5 mm
15% 5 mm
15% 5 mm
Bending
Deformation
(c)
(d)
Sample-β
Sample-α
"Columnar grain" morphology
Densely homogeneous morphology
Fully "columnar grain" morphology
Increased thermal field
Ag
Cu
O
500 μm
2mm
O:2.07% Cu:5.01% Ag:92.93% Wt%
(e)
GRX-810
AM 718
1 cm
Strength (MPa)
Tensile comparison, 1,093 °C
Creep strain (%)
Time /h
(f)
100 μm
Wood-inspired metamaterials
Polluted water
Tiny metamaterial catalyst framework
Clean water

level of control over laser scanning strategies was demonstrated by Xiong *et al.* which led to the incorporation of multiscale columnar grains, forming mesoscale gradient AgCu alloy materials, with large angle boundaries with the purpose of improving the ductility (upwards of +28%), while maintaining good conductivity properties, shown in Figure 8.5d.[72] The anisotropic properties of highly conductive metal composites have widespread implications for future electronics and thermal management devices without increased fabrication complexity.[72] High entropy alloys, alloys that contain multiple metals in packed crystal structures, exhibit superior corrosive and mechanical properties at extreme temperatures for applications that require lightweight and durable metals that are creep resistant.[73] As shown in Figure 8.5e, Smith *et al.* fabricated a specimen of CoNiCr that offered a 35% increase to tensile strength, creep resistance, and oxide resistance at temperatures around 1093 °C through the SLM approach.[73] Furthermore, Zhang *et al.* demonstrated that bioinspired designs from a Douglas fir tree could be reproduced using SLM technologies to design highly efficient water filtration metamaterials that exhibits increased mechanical performance and higher flow rates from SS 316 L and Co with microlattice features, (Figure 8.5f).[74] The potential application of SLM-printed metal nanocomposites has ushered in new perspectives within the engineering community to address emerging design challenges in extreme environments.

Figure 8.5 Recent applications in SLM-based printing approaches showing (a) crack inhibiting CoNi superalloy turbine blade, with displayed grain orientation, and columnar mechanical specimen. Scale bars are 2 cm. Reproduced from ref. 64, https://doi.org/10.1038/s41467-020-18775-0, under the terms of the CC BY 4.0 License, http://creativecommons.org/licenses/by/4.0/. (b) SEM and mechanical testing of SLM-printed CuCrZr microlattice with different volume fraction. Reproduced from ref. 70 with permission from Elsevier, Copyright 2020. (c) SEM and X-ray imaging of microlattice implanted metal hip bone. Reproduced from ref. 71, https://doi.org/10.1038/s41598-022-22292-z, under the terms of the CC BY 4.0 License, http://creativecommons.org/licenses/by/4.0/. (d) Gradient laser scanning strategies depicting mesoscale large angle boundaries and X-ray diffraction (XRD) analysis of Cu and Ag atoms within the structure. Reproduced from ref. 72, https://doi.org/10.1038/s41598-022-08182-4, under the terms of the CC BY 4.0 License, http://creativecommons.org/licenses/by/4.0/. (e) Oxidation resistance results of high entropy alloy (HEA) along with tensile strength and creep resistance mechanical test at 1093 °C. Reproduced from ref. 73, https://doi.org/10.1038/s41586-023-05893-0, under the terms of the CC BY 4.0 license, http://creativecommons.org/licenses/by/4.0/. (f) Douglas fir inspired metamaterials with aperiodic microlattice structures printed through SLM for efficient water filtration devices. Reproduced from ref. 74, https://doi.org/10.1038/s41467-024-46337-1, under the terms of the CC BY 4.0 license, http://creativecommons.org/licenses/by/4.0/.

8.4 Multiphoton Lithography

8.4.1 Overview

Multiphoton lithography, a sophisticated technique in the realm of additive manufacturing or 3D printing, operates by precisely focusing a femtosecond laser pulse onto a minuscule spot within a vat containing a specially formulated resin.[75–77] This process leverages the nonlinear optical phenomenon of two-photon absorption, wherein the focused laser induces a photochemical reaction in the resin, leading to solidification and the subsequent creation of a three-dimensional structure. Multiphoton lithography is pivotal in inducing polymerization in a photosensitive resin. When the resin absorbs two photons, it triggers a photochemical reaction leading to the polymerization of the resin at the focal point. This allows for the creation of highly detailed and complex three-dimensional microstructures with a high degree of precision and spatial resolution. The ability to control polymerization at such a fine scale makes multiphoton lithography an invaluable tool in fields requiring intricate patterns and structures. Notably, two-photon polymerization (TPP),[77] a subset of this technique, offers unparalleled resolution in the field of 3D printing, achieving feature sizes as small as approximately 50 nm.[8] This high resolution is instrumental in fabricating intricate and precise microstructures, pivotal for applications in micro-optics,[78,79] biomedical devices,[80–82] and microfluidics.[83,84]

8.4.2 The Principle and Development of the Multiphoton Lithography Process

In contrast to traditional single-photon printing methods, like stereolithography (SLA),[85,86] digital light processing (DLP),[87–90] and liquid crystal display (LCD),[91] which use higher energy ultraviolet light, multiphoton lithography (MPL) relies on multiphoton absorption, typically two-photon absorption, where two lower-energy photons (often infrared) are simultaneously absorbed to trigger polymerization. While single-photon lithography can achieve micron-level precision, it is limited by diffraction, usually to the scale of the used light's wavelength. Due to photopolymerization occurring only at the focal point of two photons and not being limited by diffraction, MLP achieves higher precision, down to about 50 nm. However, serial scanning MPL is limited by the speed of fabrication, as voxels are cured one at a time, and only one voxel is cured at any given moment, usually taking tens of hours to print a sub-millimeter 3D structure. Currently, projection MPL and parallel scanning MPL or multi-foci parallelization significantly increase manufacturing speed while maintaining precision. In projection MPL,[8] as shown in Figure 8.6a, near-infrared femtosecond (fs) pulses are generated using a laser with a broad wavelength spectrum. This light is patterned through a digital micromirror device (DMD), where the intensity of each micromirror is modulated to create high

and low states. The post-collimated light is temporally focused into the photopolymer material *via* an objective lens to form distinct cured voxels that replicate the mask's pixelated image. Three-dimensional structures are fabricated by dynamically adjusting the focal plane of sliced images within the resist, achieving a printing speed of 10^{-3} $mm^3\,s^{-1}$ for millimeter-scale 3D structures. However, projection MPL requires highly sensitive photoresins and requires lasers with high instantaneous power due to large-area two-dimensional projection. Additionally, given the non-single voxel focus, energy distribution on the two-dimensional plane becomes challenging to uniformize, hence it is often used for printing periodic and regular 3D structures. Scanning MPL effectively addresses these challenges, with single voxel scanning further improving forming precision and minimizing feature size. Highly focused energy reduces material requirements and allows more materials to be used without shape complexity limits. Its drawback is the slow fabrication speed, which limits practical utility. The recently developed multi-foci parallelization upgrades from single to multiple parallel focuses, improving printing speed to some extent. For instance, as shown in Figure 8.6b, Ouyang *et al.* developed a digital holography for parallel writing with up to 2000 foci using a 1 kHz frequency laser amplifier.[92] This ultrafast 3D nanofabrication achieves 2×10^6 voxel s^{-1} or 54 $mm^3\,h^{-1}$, with *XY* plane precision of 90 nm and *Z*-direction precision of 141 nm. Further, Jiao *et al.* combined the advantages of scanning and projection MPL to develop an eight-foci parallelization based on acoustic-optic scanning, effectively avoiding the low rate of traditional mechanical scanning, achieving a print rate of 7.6×10^7 voxel s^{-1}(Figure 8.6c).[93] In summary, multiphoton lithography has evolved from serial scanning to multi-foci parallelization and projection multiphoton lithography. These upgraded technologies have improved printing rates, precision, and manufacturing freedom to varying degrees, thereby finding broad applications in fields like optics, flexible electronics, metamaterials, and micro/nanorobots.[94–96]

8.4.3 Materials for Multiphoton Lithography

In the field of multiphoton lithography, the selection of materials plays a crucial role in determining the efficacy and scope of the fabrication process. Central to MPL are photosensitive resins, which are carefully designed to respond to two-photon absorption induced by femtosecond laser pulses. These materials predominantly include: (1) the photopolymer resins embedded with photoinitiators, which are foundational in MPL, undergoing polymerization upon exposure to femtosecond laser pulses.[97] (2) The inorganic–organic hybrid polymers that can enhance mechanical robustness and flexibility, which are especially advantageous in the situation of demanding structural resilience.[78] (3) Biocompatible polymers, which are instrumental in the fabrication of microstructures for diverse medical purposes, including tissue engineering and drug delivery systems.[80] (4) The nanocomposites that incorporate nanoparticles within the resin matrix to

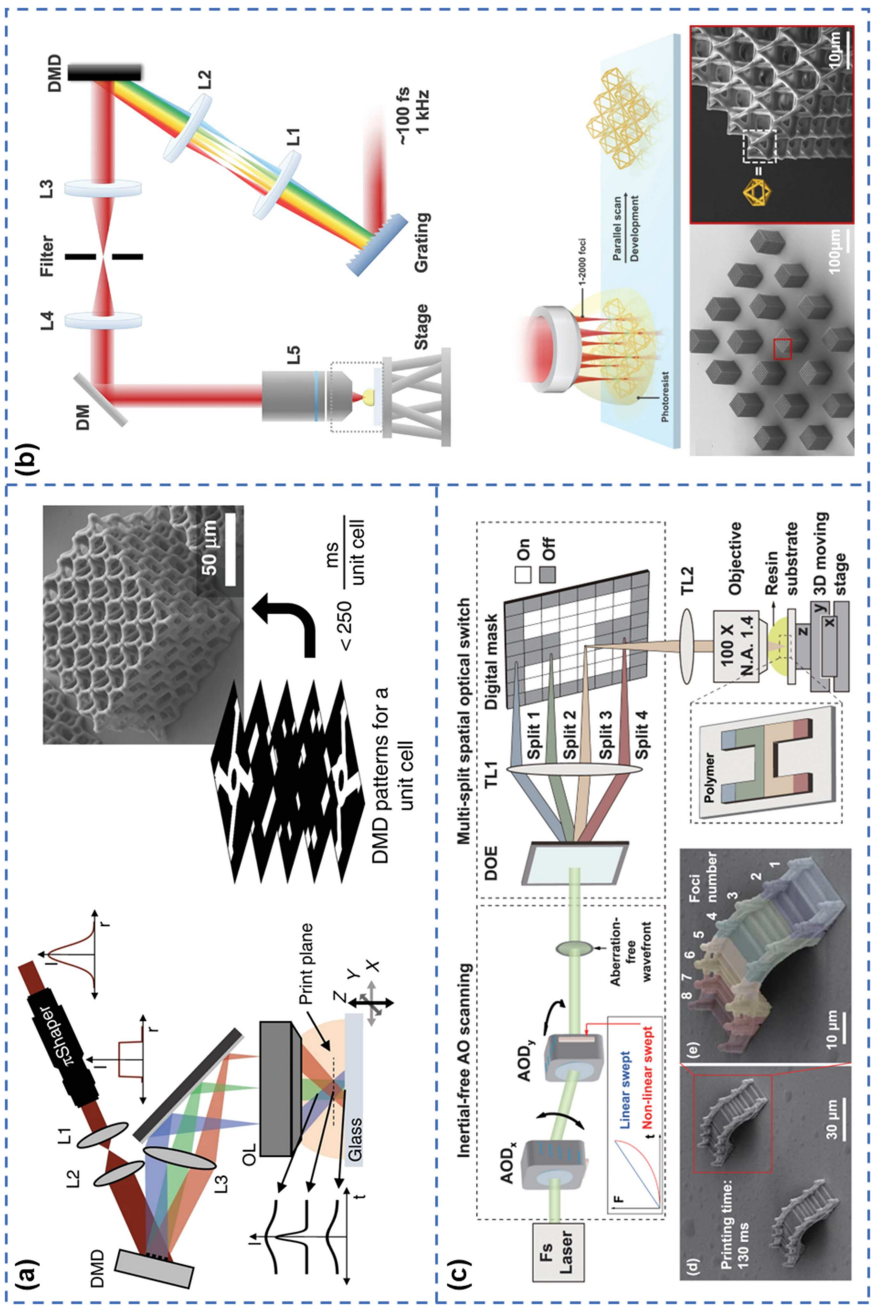
(a)
DMD
L2
L1
πShaper
L3
OL
Print plane
Glass
DMD patterns for a unit cell
50 µm
< 250 ms / unit cell
(b)
DM
L4
Filter
L3
DMD
L2
L1
L5
Stage
Grating
~100 fs
1 kHz
1-2000 foci
Parallel scan
Development
Photoresist
10µm
100µm
(c)
Inertial-free AO scanning
Multi-split spatial optical switch
Fs Laser
AOD$_x$
AOD$_y$
Aberration-free wavefront
Linear swept
Non-linear swept
DOE
TL1
Digital mask
On
Off
Split 1
Split 2
Split 3
Split 4
TL2
Objective
100 X
N.A. 1.4
Resin substrate
3D moving stage
Polymer
(d)
Printing time:
130 ms
30 µm
(e)
Foci number
10 µm

augment the functional properties of the resultant structures.[98] For instance, the integration of metallic nanoparticles can impart improved electrical or magnetic characteristics, widening MPL's utility in electronics and photonics. (5) The photochromic and electrochromic materials have the capability of altering their coloration in response to light or electrical stimuli, offer intriguing prospects for the development of responsive microstructures for advanced sensing and display technologies.[99,100] The ongoing research and development in these material categories are continuously expanding the boundaries of MPL, paving the way for its application across a spectrum of cutting-edge technological fields (Table 8.3).

8.4.4 Applications

MPL is a versatile technology widely used across various fields. Brown *et al.* utilized MPL to create flexible electrode arrays for chronic recordings in a zebra finch from structures with high surface area upwards of 0.391 mm^2, as shown in Figure 8.7a.[103] This printed electrode can record physiological signals with high temporal resolutions, crucial for biosensing applications that can easily deform and be implanted into complex anatomical structures like the human brain. In biomedical engineering, MPL is instrumental in fabricating complex tissue scaffolds and microfluidic devices for drug delivery and lab-on-a-chip systems. Maibohm *et al.* studied 3D microstructures incubating HeLa cells, finding that cell proliferation rates were faster in 3D environments compared with 2D (Figure 8.7b).[102] Similarly, Dobos *et al.* explored the migration, controlled arrangement, and degradation of L929 fibroblast cells in Gel–NB hydrogel 3D scaffolds printed using MPL (Figure 8.7c).[80] Ouyang *et al.*, as depicted in Figure 8.7d, created cubic metastructures using digital holography-based MPL, demonstrating their ability to fully recover after being compressed by 30%.[92] This method offers faster production rates, massive repeated united cells, and macroscopic mechanical properties in the final print, like effectively withstanding cyclic compression load. MPL's precision is also critical in photonics, particularly for creating micro-optical components such as waveguides and photonic crystals. Kotz *et al.* used multiphoton lithography to create a transparent sub-millimeter fused silica glass structure with a precision of several 10 μm.

Figure 8.6 Current development of multiphoton lithography. (a) Projection multiphoton lithography by spatiotemporal focusing of femtosecond pulses. Reproduced from ref. 8, https://doi.org/10.1038/s41377-021-00645-z, under the terms of the CC BY 4.0 License, https://creativecommons.org/licenses/by/4.0/. (b) Multi-foci parallelization *via* digital holography. Reproduced from ref. 92, https://doi.org/10.1038/s41467-023-37163-y, under the terms of the CC BY 4.0 License, https://creativecommons.org/licenses/by/4.0/. (c) Parallel scanning multiphoton lithography based on acousto-optic scanning with spatial-switching spots. Reproduced from ref. 93, https://doi.org/10.1088/2631-7990/ace0a7, under the terms of the CC BY 4.0 license, https://creativecommons.org/licenses/by/4.0/.

Table 8.3 Summary of recent progress in multiphoton lithography. Gel-NB, gelatin-norbornene; Gel-SH, thiolated gelatin.

Study	Method	Material	Lateral voxel size	Minimum feature size	Linear scanning/ volume speed	Application
Dadras-Toussi *et al.*[101]	Serial scanning	Poly(ethylene glycol) diacrylate		~400 nm	50 $\mu m\,s^{-1}$	Flexible electronic circuits, biosensors, bioelectronics
Maibohm *et al.*[102]	Serial scanning	S1800 series photoresist	<1 μm	~1 μm	15 $\mu m\,s^{-1}$	Cell incubation
Saha *et al.*[97]	Projection	Pentaerythritol triacrylate, bisphenol A ethoxylate diacrylate	<150 nm	175 nm	5–20 $mm^3\,h^{-1}$	Metastructures, nanowires
Kotz *et al.*[78]	Serial scanning	Resin R6-3	500 nm	~100 μm	100 $mm\,s^{-1}$	Fused silica glass, microlens array
Jiao *et al.*[93]	Multi-foci parallelization	IP-L, IP-Dip	212 nm	163 nm	2091 $mm\,s^{-1}$ or 7.6×10^7 voxel s^{-1}	Metastructures, nanowires
Dobos *et al.*[80]	Serial scanning	Gel–NB	500 nm	~10 μm	1000 $mm\,s^{-1}$	Cell culture scaffold
Somers *et al.*[8]	Projection	Pentaerythritol triacrylate	~51 nm	~200 nm	$6 \times 10^{-2} mm^3\,h^{-1}$	Microlens arrays, lattice structure
Geng *et al.*[9]	Multi-foci parallelization	IP-Dip	130 nm	~400 nm	~5 $\mu m\,s^{-1}$	Overhanging structures
Ouyang *et al.*[92]	Multi-foci parallelization	Pentaerythritol triacrylate, bisphenol A ethoxylate diacrylate	90 nm	720 nm	54 $mm^3\,h^{-1}$ or 2×10^6 voxels s^{-1}	Mechanical metamaterials, micro-lenses, magnetic micro-gear
Nishiguchi *et al.*[104]	Serial scanning	*N*-Isopropylacrylamide*N*,*N*′-methylenebis-acrylamide	150 nm	760 nm	10 $mm\,s^{-1}$	Light-driven soft actuator
Buchegger *et al.*[105]	Serial scanning	Pentaerythritol triacrylate, 2-carboxyethyl acrylate	~65 nm	~100 nm	10–20 $\mu m\,s^{-1}$	Microfluidic device
Dobos *et al.*[83]	Serial scanning	Gel-NB, Gel-SH	~500 nm	10 μm	1000 $mm\,s^{-1}$	Microvascular structures
Liu *et al.*[98]	Serial scanning	Trimethylopropane triacrylate, pentaerythritol triacrylate	~100 nm	300 nm	10000 $mm\,s^{-1}$	3D nanocomposite structures

The surface roughness of the sintered silica microlens array can be as low as about 6 nm, proving that the printing and sintering process has significant applications in the field of optics (Figure 8.7e).[78] Jiao *et al.* developed acousto-optic scanning with spatial-switching multispots MPL for manufacturing complex 3D microstructures, ensuring structural complexity with parallel material curing and high precision (Figure 8.7f).[93] MPL is also essential in developing microelectromechanical systems (MEMS) and contributes to material science, aerospace, and automotive industries, besides unique applications in the arts.[75,76]

8.5 Outlook and Perspectives

8.5.1 Selective Laser Sintering

Selective laser sintering has paved the way for using advanced ceramic and polymer composites to produce complex geometries with enhanced performance from the fusion of nanocomposite powders. SLS technologies have made use of scanning lasers to fabricate hierarchical components with macroscale to microscale resolution with promising applications in biomedicine, electronics, and flexible sensors. The main limitation of the SLS process is that the equipment cost and required processing steps are expensive and require specialized equipment to maintain the atmospheric conditions. Furthermore, the surface roughness of sintered samples is extremely poor since the energy deposition induced by the laser causes significant thermal gradients and particle ejection that result in surface defects. Post-processing steps, such as milling and polishing, have been explored to mitigate the surface roughness issue. However, more work needs to be done in order to address control of morphologies on the microscale. Moreover, the laser scanning process to construct the 3D object is often time consuming since the tool must trace and fill in the entire layer before moving forward, in comparison to powder binding in which a whole layer is cured instantaneously. The perspectives of SLS-printed components are auspicious and future research directives aim to address current challenges and limitations. The primary objective of recent work is to investigate the particle sintering kinetics to control thermal effects from laser deposition on the surface and powder processing to expand the library of nanocomposite materials capable of being printed using SLS. Certain nanofillers must be carefully processed in order to ensure that the merging during powder sintering is efficient and mitigates crack formation from anisotropic shrinkage. Overall, the potential application for SLS in prominent engineering design challenges is expected to increase.

8.5.2 Selective Laser Melting

Selective laser melting technology has expanded upon the field of metals and metal matrix composite fabrication leading to innovative solutions in the

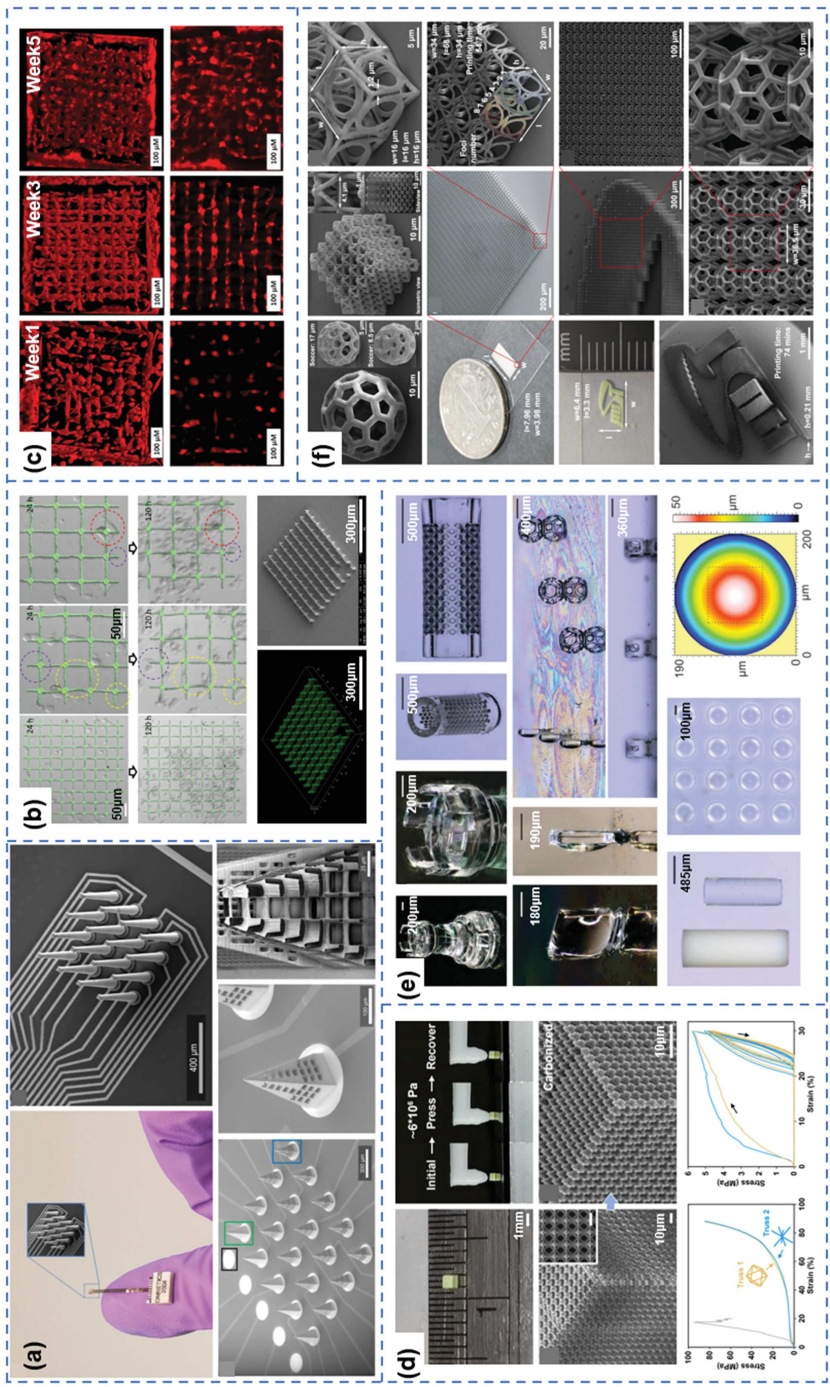
(a)
400 μm
(b)
24 h
120 h
50μm
300μm
(c)
Week1
Week3
Week5
100 μM
(d)
~6*10⁴ Pa
Initial → Press → Recover
1mm
10μm
Carbonized
Truss 1
Truss 2
Stress (MPa)
Strain (%)
(e)
200μm
500μm
190μm
180μm
360μm
100μm
485μm
(f)
Printing time: 74 mins
5 mm
20 μm
100 μm
10 μm

chemical and aerospace industries. The scanning strategies and utilization of a high-power laser to selectively melt metal composites opens up new methods for designing highly efficient turbine blades and automotive components capable of withstanding the most extreme environments. The major limitation of SLM printing is complexity and cost associated with the necessary powder processing, environmental control, and laser optical system, in addition to post-processing, involved in the manufacturing process. Furthermore, laser optical systems and composite powders are inherently dangerous and require specialized equipment that may not be easily procured. Furthermore, the resolution of the printed parts is constrained by the laser scanning distance and spot diameter and results in poor surface roughness through the energy deposition process *via* large thermal induced stresses and particle ejection, resulting in surface defects in the final printed part. The laser tool path is also limited by the scanning speed and area fabrication which increases the build time for macroscale components. Since recent work on the SLM approach has demonstrated the ability to fabricate high entropy alloys and metal–ceramic structures with unique morphology, numerous studies focused on mitigating these issues and risks have been performed. Advances in laser technologies have enabled the use of unique laser scanning strategies to develop grain boundaries that deflect shearing forces, leading to improved mechanical strength and ductility. Furthermore, new super alloys and nanocomposites can be fabricated through this facile AM approach to enhance corrosion resistance for oxidation- and fatigue-resistant materials with high strength. Therefore, the SLM process is set to contribute greatly to manufacturing advances in the nuclear, turbomachinery, and aerospace sectors over the next decade.

Figure 8.7 Application of multiphoton lithography. (a) Multiphoton lithography of a 16-electrode array with high surface area for electrophysiological sensing in small animals. Reproduced from ref. 103, https://doi.org/10.1038/s41467-023-39152-7, under the terms of the CC BY 4.0 license, https://creativecommons.org/licenses/by/4.0/. (b) 2D and 3D microstructures for cell culture. Reproduced from ref. 102, https://doi.org/10.1038/s41598-020-64955-9, under the terms of the CC BY 4.0 license, http://creativecommons.org/licenses/by/4.0/. (c) Multiphoton lithography of 3D scaffold with degradable hydrogel. Reproduced from ref. 80, https://doi.org/10.1002/adhm.201900752, under the terms of the CC BY 4.0 license, https://creativecommons.org/licenses/by/4.0/. (d) Scalable manufacturing of metastructures with bulky mechanical properties. Reproduced from ref. 92, https://doi.org/10.1038/s41467-023-37163-y, under the terms of the CC BY 4.0 license, https://creativecommons.org/licenses/by/4.0/. (e) Multiphoton lithography of fused transparent silica glass. Reproduced from ref. 78, https://doi.org/10.1002/adma.202006341, under the terms of the CC BY 4.0 license, https://creativecommons.org/licenses/by/4.0/. (f) Cross-scale manufacturing of metastructures with complex unit cells. Reproduced from ref. 93, https://doi.org/10.1088/2631-7990/ace0a7, under the terms of the CC BY 4.0 license, https://creativecommons.org/licenses/by/4.0/.

8.5.3 Multiphoton Lithography

Multiphoton lithography represents a cutting-edge approach in the realm of microfabrication, characterized by its use of nonlinear two-photon absorption techniques. MPL leverages the precision of femtosecond laser pulses and facilitates the creation of complex three-dimensional microstructures with nanoscale resolution. MPL is renowned for its ability to fabricate intricate geometries, making it invaluable in fields such as microoptics, biomedicine, and microfluidics. One of the primary challenges of MPL is the substantial cost and complexity associated with its necessary equipment, particularly femtosecond laser systems. The technique also faces limitations in terms of the variety of materials that can be effectively utilized, which currently restricts its broader application. Furthermore, the inherent nature of the point-by-point writing process integral to MPL results in relatively slow fabrication speeds, posing a significant hindrance to its efficiency and scalability. Looking forward, the outlook for MPL is promising, with numerous research initiatives aimed at addressing its current limitations. The first is to break through the diffraction limit to create features of several nanometers, and the second is to manufacture three-dimensional structures with complex shapes across scales and in mass production while ensuring fine feature sizes. Efforts are being made to enhance the speed of the fabrication process, potentially through the integration of more advanced laser systems or the development of novel scanning techniques. The expansion of the range of compatible materials is also a critical area of focus, which could substantially widen the applicability of MPL. Technological advancements in laser engineering and photoresist development are anticipated to play a pivotal role in overcoming existing challenges, thereby broadening the scope of MPL's applications in various sectors demanding high-precision and intricate manufacturing capabilities.

References

1. H. Guo, R. Lv and S. Bai, Recent advances on 3D printing graphene-based composites, *Nano Mater. Sci.*, 2019, **1**(2), 101–115.
2. Gan, X., *et al.*, Powder quality and electrical conductivity of selective laser sintered polymer composite components, in *Structure and Properties of Additive Manufactured Polymer Components*, 2020, Elsevier, pp. 149-185.
3. Q.-P. Ma, *et al.*, Residual Stress Build-Up in Aluminum Parts Fabricated with SLM Technology Using the Bridge Curvature Method, *Materials*, 2022, **15**(17), 6057.
4. S. Lekurwale, T. Karanwad and S. Banerjee, Selective laser sintering (SLS) of 3D printlets using a 3D printer comprised of IR/red-diode laser. Annals of 3D Printed, *Medicine*, 2022, **6**, 100054.
5. F. Fina, *et al.*, Selective laser sintering (SLS) 3D printing of medicines, *Int. J. Pharm.*, 2017, **529**(1–2), 285–293.

6. A. Moridi, *et al.*, Deformation and failure mechanisms of Ti–6Al–4V as built by selective laser melting, *Mater. Sci. Eng., A*, 2019, **768**, 138456.
7. P. Mohyla, *et al.*, Analysis of welded joint properties on an AISI316L stainless steel tube manufactured by SLM technology, *Materials*, 2020, **13**(19), 4362.
8. P. Somers, *et al.*, Rapid, continuous projection multi-photon 3D printing enabled by spatiotemporal focusing of femtosecond pulses, *Light: Sci. Appl.*, 2021, **10**(1), 199.
9. Q. Geng, *et al.*, Ultrafast multi-focus 3-D nano-fabrication based on two-photon polymerization, *Nat. Commun.*, 2019, **10**(1), 2179.
10. G. Rollo, *et al.*, On the synergistic effect of multi-walled carbon nanotubes and graphene nanoplatelets to enhance the functional properties of SLS 3D-printed elastomeric structures, *Polymers*, 2020, **12**(8), 1841.
11. H. Naujokat, *et al.*, In vivo biocompatibility evaluation of 3D-printed nickel–titanium fabricated by selective laser melting, *J. Mater. Sci.: Mater. Med.*, 2022, **33**(2), 13.
12. N. Alinejadian, S. H. Kazemi and I. Odnevall, SLM-processed MoS_2/Mo_2S_3 nanocomposite for energy conversion/storage applications, *Sci. Rep.*, 2022, **12**(1), 5030.
13. E. Johlin, *et al.*, Broadband highly directive 3D nanophotonic lenses, *Nat. Commun.*, 2018, **9**(1), 4742.
14. E. Kabouraki, *et al.*, High laser induced damage threshold photoresists for nano-imprint and 3D multi-photon lithography, *Nanophotonics*, 2021, **10**(14), 3759–3768.
15. Q. Chen, *et al.*, Three-dimensional finite element thermomechanical modeling of additive manufacturing by selective laser melting for ceramic materials, *Addit. Manuf.*, 2017, **16**, 124–137.
16. L. Constantin, *et al.*, Laser 3D printing of complex copper structures, *Addit. Manuf.*, 2020, **35**, 101268.
17. P. Hejmady, *et al.*, Laser sintering of PA12 particles studied by in situ optical, thermal and X-ray characterization., *Addit. Manuf.*, 2022, **52**, 102624.
18. M. Zhou, *et al.*, Selective laser sintering of carbon nanotube–coated thermoplastic polyurethane: Mechanical, electrical, and piezoresistive properties, *Compos., Part C: Open Access*, 2022, **7**, 100212.
19. N. A. Charoo, *et al.*, Selective laser sintering 3D printing–an overview of the technology and pharmaceutical applications, *Drug Dev. Ind. Pharm.*, 2020, **46**(6), 869–877.
20. P. Navarrete-Segado, *et al.*, Powder bed selective laser process (sintering/melting) applied to tailored calcium phosphate-based powders, *Addit. Manuf.*, 2022, **50**, 102542.
21. S. J. Trenfield, *et al.*, Releasing fast and slow: Non-destructive prediction of density and drug release from SLS 3D printed tablets using NIR spectroscopy, *Int. J. Pharm.: X*, 2023, **5**, 100148.
22. G. Wang, *et al.*, Preparation of PA12 microspheres with tunable morphology and size for use in SLS processing, *Mater. Des.*, 2015, **87**, 656–662.

23. S. Chang, *et al.*, Selective laser sintering of porous silica enabled by carbon additive, *Materials*, 2017, **10**(11), 1313.
24. B. Chen, *et al.*, Laser sintering of graphene nanoplatelets encapsulated polyamide powders, *Addit. Manuf.*, 2020, **35**, 101363.
25. S. Song, *et al.*, Boosting piezoelectric performance with a new selective laser sintering 3D printable PVDF/graphene nanocomposite, *Composites, Part A*, 2021, **147**, 106452.
26. B. Ding, *et al.*, Selective laser sintering 3D-Printed conductive thermoplastic polyether-block-amide elastomer/carbon nanotube composites for strain sensing system and electro-induced shape memory, *Compos. Commun.*, 2022, **35**, 101280.
27. A. Mazzoli, G. Moriconi and M. G. Pauri, Characterization of an aluminum-filled polyamide powder for applications in selective laser sintering, *Mater. Des.*, 2007, **28**(3), 993–1000.
28. F. Qi, N. Chen and Q. Wang, Dielectric and piezoelectric properties in selective laser sintered polyamide11/$BaTiO_3$/CNT ternary nanocomposites, *Mater. Des.*, 2018, **143**, 72–80.
29. C. Gómez-Rodríguez, *et al.*, Selective laser sintering of alumina-molybdenum nanocomposites, *Ceram. Int.*, 2022, **48**(19), 29540–29545.
30. M. Li, *et al.*, Lightweight mullite ceramics with controlled porosity and enhanced properties prepared by SLS using mechanical mixed FAHSs/polyamide12 composites, *Ceram. Int.*, 2019, **45**(16), 20803–20809.
31. S. Yuan and X. Yu, Ultrasonic non-destructive evaluation of selectively laser-sintered polymeric nanocomposites, *Polym. Test.*, 2020, **90**, 106705.
32. F. Taher, *et al.*, Enhancing the tensile properties of PA6/CNT nanocomposite in selective laser sintering process, *Polym. Compos.*, 2023, **44**(2), 1290–1304.
33. S. Yu, *et al.*, Preparation and electromagnetic wave absorption properties of PDC–SiC/Si_3N_4 composites using selective laser sintering and infiltration technology, *J. Mater. Res. Technol.*, 2023, **23**, 2888–2899.
34. C. Wang, *et al.*, 3D printed porous biomass–derived SiCnw/SiC composite for structure–function integrated electromagnetic absorption, *Virtual Phys. Prototyping*, 2022, **17**(3), 718–733.
35. L. Lanzl, *et al.*, Selective laser sintering of copper filled polyamide 12: Characterization of powder properties and process behavior, *Polym. Compos.*, 2019, **40**(5), 1801–1809.
36. K. A. Ibrahim, B. Wu and N. P. Brandon, Electrical conductivity and porosity in stainless steel 316L scaffolds for electrochemical devices fabricated using selective laser sintering, *Mater. Des.*, 2016, **106**, 51–59.
37. I. S. Kinstlinger, *et al.*, Open-source selective laser sintering (OpenSLS) of nylon and biocompatible polycaprolactone, *PLoS One*, 2016, **11**(2), e0147399.
38. T. Qin, *et al.*, Bioactive tetracalcium phosphate scaffolds fabricated by selective laser sintering for bone regeneration applications, *Materials*, 2020, **13**(10), 2268.

39. N. Roy, *et al.*, A novel microscale selective laser sintering (μ-SLS) process for the fabrication of microelectronic parts, *Microsyst. Nanoeng.*, 2019, **5**, 64.
40. I. Yadroitsev, P. Krakhmalev and I. Yadroitsava, Hierarchical design principles of selective laser melting for high quality metallic objects, *Addit. Manuf.*, 2015, **7**, 45–56.
41. N. Omidi, P. Farhadipour and N. Barka, Investigation into the effect of the SLM processing parameters on the microstructure and mechanical behavior of M300; experimental and statistical analysis, *Int. J. Adv. Manuf. Technol.*, 2023, 1–16.
42. H.-C. Tran and Y.-L. Lo, Heat transfer simulations of selective laser melting process based on volumetric heat source with powder size consideration, *J. Mater. Process. Technol.*, 2018, **255**, 411–425.
43. A. E. Jakus, *et al.*, Metallic architectures from 3D-printed powder-based liquid inks, *Adv. Funct. Mater.*, 2015, **25**(45), 6985–6995.
44. G. Kasperovich and J. Hausmann, Improvement of fatigue resistance and ductility of $TiAl_6V_4$ processed by selective laser melting, *J. Mater. Process. Technol.*, 2015, **220**, 202–214.
45. E. Li, *et al.*, Particle scale modelling of melt pool dynamics and pore formation in selective laser melting additive manufacturing, *Powder Technol.*, 2022, **397**, 117012.
46. X. Liu, *et al.*, CNT-reinforced AlSi10Mg composite by selective laser melting: microstructural and mechanical properties, *Mater. Sci. Technol.*, 2019, **35**(9), 1038–1045.
47. Y. Liu, *et al.*, Processing and properties of topologically optimised biomedical Ti–24Nb–4Zr–8Sn scaffolds manufactured by selective laser melting, *Mater. Sci. Eng., A*, 2015, **642**, 268–278.
48. Y. Zhou, K. Zhang, Y. Liang, J. Cheng and Y. Dai, Selective Laser Melted Magnesium Alloys: Fabrication, Microstructure and Property, *Materials*, 2022, **15**(20), 7049.
49. C. Meier, *et al.*, Critical influences of particle size and adhesion on the powder layer uniformity in metal additive manufacturing, *J. Mater. Process. Technol.*, 2019, **266**, 484–501.
50. H. Zhang, *et al.*, Manufacturing and analysis of high-performance refractory high-entropy alloy via selective laser melting (SLM), *Materials*, 2019, **12**(5), 720.
51. L. Constantin, *et al.*, Manufacturing of complex diamond-based composite structures via laser powder-bed fusion, *Addit. Manuf.*, 2021, **40**, 101927.
52. D. Zhang, *et al.*, In situ observation of crystal rotation in Ni-based superalloy during additive manufacturing process, *Nat. Commun.*, 2023, **14**(1), 2961.
53. Q. Han, R. Setchi and S. L. Evans, Synthesis and characterisation of advanced ball-milled Al-Al_2O_3 nanocomposites for selective laser melting, *Powder Technol.*, 2016, **297**, 183–192.

54. B. AlMangour, D. Grzesiak and J.-M. Yang, In situ formation of TiC-particle-reinforced stainless steel matrix nanocomposites during ball milling: Feedstock powder preparation for selective laser melting at various energy densities, *Powder Technol.*, 2018, **326**, 467–478.
55. Z. Zhu, *et al.*, Selective laser melting enabling the hierarchically heterogeneous microstructure and excellent mechanical properties in an interstitial solute strengthened high entropy alloy, *Mater. Res. Lett.*, 2019, **7**(11), 453–459.
56. X. Yao, *et al.*, Effects of heat treatment on microstructures and tensile properties of IN718/TiC nanocomposite fabricated by selective laser melting, *Int. J. Precis. Eng. Manuf.*, 2017, **18**, 1693–1701.
57. S. Luo, *et al.*, Selective laser melting of dual phase AlCrCuFeNix high entropy alloys: Formability, heterogeneous microstructures and deformation mechanisms, *Addit. Manuf.*, 2020, **31**, 100925.
58. J. J. Marattukalam, *et al.*, The effect of laser scanning strategies on texture, mechanical properties, and site-specific grain orientation in selective laser melted 316L SS, *Mater. Des.*, 2020, **193**, 108852.
59. L. Jiang, *et al.*, Preparation and mechanical properties of CNTs-AlSi10Mg composite fabricated via selective laser melting, *Mater. Sci. Eng., A*, 2018, **734**, 171–177.
60. N. Alinejadian, *et al.*, Importance of the micro-lattice structure of selective laser melting processed Mo/Mo(x)S(x+1) composite: Corrosion studies on the electrochemical performance in aqueous solutions. Materials Today, *Chemistry*, 2022, **26**, 101219.
61. M. S. Dargusch, *et al.*, Exploring the role of manganese on the microstructure, mechanical properties, biodegradability, and biocompatibility of porous iron-based scaffolds, *ACS Biomater. Sci. Eng.*, 2019, **5**(4), 1686–1702.
62. J. Hu, X. Lin and Y. Hu, High wear resistance and strength of Hastelloy X reinforced with TiC fabricated by laser powder bed fusion additive manufacturing, *Appl. Surf. Sci.*, 2023, 159004.
63. A. Golyshev, *et al.*, The effect of using repetitively pulsed laser radiation in selective laser melting when creating a metal-matrix composite Ti-6Al-4V–B 4 C, *Int. J. Adv. Manuf. Technol.*, 2021, **117**, 1891–1904.
64. S. P. Murray, *et al.*, A defect-resistant Co–Ni superalloy for 3D printing, *Nat. Commun.*, 2020, **11**(1), 4975.
65. A. Baroutaji, *et al.*, The Influence of Atmospheric Oxygen Content on the Mechanical Properties of Selectively Laser Melted AlSi10Mg TPMS-Based Lattice, *Materials*, 2023, **16**(1), 430.
66. N. Kang, *et al.*, Microstructure and wear properties of selective laser melted WC reinforced 18Ni-300 steel matrix composite, *Vacuum*, 2018, **154**, 69–74.
67. C. Xin, *et al.*, Microstructure, grain and nanowire growth during selective laser melting of Ag–Cu/diamond composites, *RSC Adv.*, 2023, **13**(6), 3448–3458.

68. A. Davydova, *et al.*, Selective laser melting of boron carbide particles coated by a cobalt-based metal layer, *J. Mater. Process. Technol.*, 2016, **229**, 361–366.
69. S. Wen, *et al.*, Selective laser melting of reduced graphene oxide/S136 metal matrix composites with tailored microstructures and mechanical properties, *Mater. Des.*, 2019, **175**, 107811.
70. Z. Ma, *et al.*, Lattice structures of Cu-Cr-Zr copper alloy by selective laser melting: Microstructures, mechanical properties and energy absorption, *Mater. Des.*, 2020, **187**, 108406.
71. J. W. Park, *et al.*, Fabrication of a lattice structure with periodic open pores through three-dimensional printing for bone ingrowth, *Sci. Rep.*, 2022, **12**(1), 17223.
72. W. Xiong, *et al.*, Simultaneous strength and ductility enhancements of high thermal conductive Ag7. 5Cu alloy by selective laser melting, *Sci. Rep.*, 2022, **12**(1), 4250.
73. T. M. Smith, *et al.*, A 3D printable alloy designed for extreme environments, *Nature*, 2023, 1–6.
74. L. Zhang, H. Liu, B. Song, J. Gu, L. Li, W. Shi, G. Li, S. Zhong, H. Liu, X. Wang and J. Fan, Wood-inspired metamaterial catalyst for robust and high-throughput water purification, *Nat. Commun.*, 2024, **15**(1), 2046.
75. V. Harinarayana and Y. C. Shin, Two-photon lithography for three-dimensional fabrication in micro/nanoscale regime: A comprehensive review, *Opt. Laser Technol.*, 2021, **142**, 107180.
76. H. Wang, *et al.*, Two-Photon Polymerization Lithography for Optics and Photonics: Fundamentals, Materials, Technologies, and Applications, *Adv. Funct. Mater.*, 2023, **33**(39), 2214211.
77. V. Hahn, *et al.*, Rapid Assembly of Small Materials Building Blocks (Voxels) into Large Functional 3D Metamaterials, *Adv. Funct. Mater.*, 2020, **30**(26), 1907795.
78. F. Kotz, *et al.*, Two-Photon Polymerization of Nanocomposites for the Fabrication of Transparent Fused Silica Glass Microstructures, *Adv. Mater.*, 2021, **33**(9), 2006341.
79. Y. Zhu, *et al.*, Recent advancements and applications in 3D printing of functional optics, *Addit. Manuf.*, 2022, **52**, 102682.
80. A. Dobos, *et al.*, Thiol–Gelatin–Norbornene Bioink for Laser-Based High-Definition Bioprinting, *Adv. Healthcare Mater.*, 2020, **9**(15), 1900752.
81. J. L. Connell, *et al.*, 3D printing of microscopic bacterial communities, *Proc. Natl. Acad. Sci. U. S. A.*, 2013, **110**(46), 18380–18385.
82. G. Flamourakis, *et al.*, Low-autofluorescence, transparent composite for multiphoton 3D printing, *Opt. Mater. Express*, 2021, **11**(3), 801–813.
83. A. Dobos, *et al.*, On-chip high-definition bioprinting of microvascular structures, *Biofabrication*, 2021, **13**(1), 015016.
84. Q. He, *et al.*, Review on 3D Printing of Bioinspired Structures for Surface/Interface Applications, *Advanced Functional Materials*, 2024, 2309323.

85. D. Joralmon, *et al.*, Three-Dimensional Printing of Liquid Crystals with Thermal Sensing Capability via Multimaterial Vat Photopolymerization, *ACS Appl. Polym. Mater.*, 2022, **4**(4), 2951–2959.
86. T. Tang, G. S. K. A. R. Dwarampudi and X. Li, Electrically Assisted Vat Photopolymerization of Bioinspired Hierarchical Structures with Controllable Roughness for Hydrophobicity Enhancement Using Photocurable Resin/Carbon Nanotube, *JOM*, 2023, **75**(7), 2137–2148.
87. L. Tiwari, *et al.*, Thermoelectric Material Fabrication using Mask Image Projection Based Stereolithography Integrated with Hot Pressing, *J. Mater. Sci. Technol. Res.*, 2022, **9**(1), 105–113.
88. T. Tang, B. Ahire and X. Li, Scalable Multi-Material Additive Manufacturing of Bioinspired Polymeric Material With Metallic Structures Via Electrically Assisted Stereolithography, *J. Manuf. Sci. Eng.*, 2022, **145**(1), 011004.
89. T. Tang, *et al.*, 4D Printing of Seed Capsule-Inspired Hygro-Responsive Structures via Liquid Crystal Templating-Assisted Vat Photopolymerization, *Adv. Funct. Mater.*, 2023, **33**(5), 2211602.
90. T. Tang, *et al.*, 4D Printing of Seed Capsule-Inspired Hygro-Responsive Structures via Liquid Crystal Templating-Assisted Vat Photopolymerization (Adv. Funct. Mater. 5/2023), *Adv. Funct. Mater.*, 2023, **33**(5), 2370029.
91. I. Roohani, A. Entezari and H. Zreiqat, Liquid crystal display technique (LCD) for high resolution 3D printing of triply periodic minimal surface lattices bioceramics, *Addit. Manuf.*, 2023, **74**, 103720.
92. W. Ouyang, *et al.*, Ultrafast 3D nanofabrication via digital holography, *Nat. Commun.*, 2023, **14**(1), 1716.
93. B. Jiao, *et al.*, Acousto-optic scanning spatial-switching multiphoton lithography, *Int. J. Extreme Manuf.*, 2023, **5**(3), 035008.
94. Tengteng, T., J. Dylan, and L. Xiangjia, 3D Printing of Biomimetic Functional Nanocomposites Via Vat Photopolymerization, in *Advances in 3D Printing*, ed. S. Ashutosh, 2023, IntechOpen, Rijeka, ch. 5.
95. Y. Zhu, *et al.*, Characterization of PEDOT:PSS Nanofilms Printed via Electrically Assisted Direct Ink Deposition with Ultrasonic Vibrations, *Molecules*, 2023, **28**(20), 7109.
96. T. Tang, *et al.*, Acoustic Levitation-Assisted Contactless Printing of Microdroplets for Biomedical Applications, *J. Manuf. Sci. Eng.*, 2023, **146**(1), 011002.
97. S. K. Saha, *et al.*, Scalable submicrometer additive manufacturing, *Science*, 2019, **366**(6461), 105–109.
98. Y. Liu, *et al.*, Additive Manufacture of Three Dimensional Nanocomposite Based Objects through Multiphoton Fabrication, *Polymers*, 2016, **8**(9), 325.
99. D. J. Wales, *et al.*, 3D-Printable Photochromic Molecular Materials for Reversible Information Storage, *Adv. Mater.*, 2018, **30**(26), 1800159.
100. S. Ulrich, *et al.*, Nano-3D-Printed Photochromic Micro-Objects, *Small*, 2021, **17**(26), 2101337.

101. O. Dadras-Toussi, *et al.*, Multiphoton Lithography of Organic Semiconductor Devices for 3D Printing of Flexible Electronic Circuits, Biosensors, and Bioelectronics, *Adv. Mater.*, 2022, **34**(30), 2200512.
102. C. Maibohm, *et al.*, Multi-beam two-photon polymerization for fast large area 3D periodic structure fabrication for bioapplications, *Sci. Rep.*, 2020, **10**(1), 8740.
103. M. A. Brown, K. M. Zappitelli, L. Singh, R. C. Yuan, M. Bemrose, V. Brogden, D. J. Miller, M. C. Smear, S. F. Cogan and T. J. Gardner, Direct laser writing of 3D electrodes on flexible substrates, *Nat. Commun.*, 2023, **14**(1), 3610.
104. A. Nishiguchi, *et al.*, 4D Printing of a Light-Driven Soft Actuator with Programmed Printing Density, *ACS Appl. Mater. Interfaces*, 2020, **12**(10), 12176–12185.
105. B. Buchegger, *et al.*, STED lithography in microfluidics for 3D thrombocyte aggregation testing, *J. Nanobiotechnol.*, 2021, **19**(1), 23.